THE INFLUENCE OF THE LENS MODEL ON TIME DELAY DURING STRONG LENSING BY GALAXIES

LINDITA HAMOLLI[1], ESMERALDA GULIQANI[2] ,

MIMOZA HAFIZI[3]

[1,3]Department of Physics, Faculty of Natural Sciences, University of Tirana

[2]Department of Mathematics and Physics, Faculty of Natural and Human Sciences, "Fan S. Noli" University of Korça

e-mail: lindita.hamolli@fshn.edu.al

Abstract

This study investigates the impact of the galactic mass distribution on the time delays between lensed images of quasars, which is a crucial method for constraining the cosmological parameters. To this aim, two models for the lens galaxy, the Singular Isothermal Sphere (SIS) and Nonsingular Isothermal Sphere (NIS), are considered. We develop a Monte Carlo simulation to investigate the probability of a quasar to be lensed only by a foreground galaxy and the time delay between lensed images. Based on the capabilities of the Roman Space telescope, using the mass-luminosity distribution function of galaxies and the redshift distribution of both galaxies and quasars, we find that 85% of the lensed quasars are lensed by a single galaxy. Further on, we find that the time delays between lensed images vary from a few hours to a few years, with the most common duration of 10 days and the influence of these two models in time delays is not very distinct.

Key words**:** *quasar, galaxy, strong lensing, time delay.*

Përmbledhje

Ky punim heton ndikimin e shpërndarjes së masës galaktike në vonesat kohore midis imazheve të lensuar të kuasarëve, e cila është një metodë thelbësore për studimin e parametrave kozmologjikë. Për këtë qëllim janë marrë në konsideratë dy modele për lentet galaktike, Singular Isothermal Sphere (SIS) dhe Nonsingular Isothermal Sphere (NIS). Për të gjetur se sa është probabiliteti që një kuazari të lensohet vetëm nga një galaksi dhe vonesën

kohore midis imazheve të lensuar kemi përdorur simulimet Monte Carlo. Bazuar në aftësitë e teleskopit hapësinor Roman, duke përdorur funksionin e shpërndarjes së mass-luminosity të galaksive dhe shpërndarjen e redshifteve të galaksive dhe të kuazarëve, kemi gjetur se 85% e kuazarëve të lensuar janë lensuar vetëm nga një galaksi e vetme. Më tej, kemi gjetur se vonesat kohore midis imazheve të lensuar variojnë nga disa orë në disa vjet, me kohëzgjatjen më të zakonshme prej 10 ditësh dhe ndikimi i këtyre dy modeleve në vonesat kohore nuk është shumë i dallueshëm.

Fjalë kyçe: *kuazar, galaksi, lensimi i fortë, vonesa kohore.*

Introduction

Gravitational lensing is the deflection of light from a distant source by the gravity of a massive object close to the line of sight. Strong lensing is the scenario when the source (quasar) appears as multiple images, amplified, or distorted into an arc-like form around a lens (foreground galaxy). Gravitational lensing is the best tool for mapping dark matter distribution and confirming the values of cosmological parameters, like the Hubble constant (H_0), because it is only dependent on the configuration and geometry of foreground matter (Schechter, 2002).

A well-known disparity exists today between the reported values of H_0. The value obtained from the distance ladder method with type Ia supernovae and Cepheids, as reported by the SH0ES team (Riess et al., 2021), is significantly different from the Planck (ΛCDM) result obtained from Cosmic Microwave Background (CMB) observations (Aiola et al., 2020; Aghanim et al., 2020). Measuring the time delays between lensed images at lensed quasars is another technique (Wong et al., 2020) that is totally independent of both supernovae and CMB.

The light rays from a distant source will take some time to reach the observer. This time depends on the potential of the gravitational field in which the bent ray propagates (Refsdal, 1964) as well as the geometrical distance that the rays must travel to get to the observer.

There are currently more than 200 known lensed quasars[3] found by different cosmological surveys, such as the Cosmic Lens All Sky Survey (CLASS), (Myers et al., 2003) or the Sloan Digital Sky Survey (SDSS), (York et al., 2000), which have provided a huge amount of photometric and spectroscopic

1/*https://research.ast.cam.ac.uk/lensedquasars/*

data. Moreover, future surveys like the Nancy Grace Roman Space Telescope (Spergel et al., 2015) and the Vera Rubin Observatory's Legacy Survey of Space and Time (LSST) are expected to quickly increase this number.

The Roman Space Telescope (Roman), formerly known as the Wide Field InfraRed Survey (WFIRST) (Spergel et al., 2015), is a NASA infrared space telescope. It is scheduled to launch in May 2027 and will be positioned at the second Lagrange point (L2) of the Earth-Sun system. Its primary goal is to investigate the nature of dark energy with a variety of methods. This will be achieved using two instruments: the Wide Field Instrument (WFI) and the Coronagraph Instrument. The WFI is equipped with eight filter band passes spanning 0.48 – 2.3 μm. The Roman survey is intended to cover 2,000 square degrees over a five year period, with a goal to extend this to ten years[4]. It has an angular resolution of about 0.11 arcsec.

The purpose of this work is to investigate the influence of the lens mass density distribution on the time delays between lensed images in the lensed quasars expected to be observed by the Roman. Quasars are distant active galactic nuclei with high intrinsic brightness and are crucial for understanding the universe structure and evolution. We are focused on systems lensed by a single galaxy considering for them two different models: the Singular Isothermal Sphere (SIS) and Nonsingular Isothermal Sphere (NIS) (Hurtado et al., 2014).

The paper structure is as follows: Section 2 provides a review of the fundamentals of gravitational lensing and discusses the determination of time delays between lensed images. In Section 3, we describe our algorithm for simulating strong lensing events and present our results. Section 4 summarizes the main conclusions. The Appendixes A and B provide additional details for both the SIS and NIS models.

Time Delay in strong lensing

Gravitational lensing is a phenomenon where light rays from a distant source are deflected by the gravitational field of the intervening objects. This effect is particularly visible in strong lensing, where light from a background source can traverse vast distances to reach the observer, resulting in multiple images of the same source. In this case, the spatial extent of the lens can often be considered negligible, leading to the “thin” lens approximation (Schneider et

[4] *https://roman.gsfc.nasa.gov/science/observatory_technical.html*

al. 1992). Consequently, the mass of the lens is projected onto a two-dimensional plane orthogonal to the line of sight.

Defining: $\vec{\beta}$ -the actual angular position of the source, $\vec{\theta}$ - the angular position of the light rays that intersect the lens plane and $\vec{\alpha}\left(\vec{\theta}\right)$ - the scaled deflection angle, the lens equation can be written as (Meylan et al., 2006),

$$\vec{\beta} = \vec{\theta} - \vec{\alpha}\left(\vec{\theta}\right). \tag{1}$$

Last term is related to the deflection angle by $\vec{\alpha}\left(\vec{\theta}\right) = \frac{D_{LS}}{D_S}\vec{\hat{\alpha}}\left(\vec{\theta}\right)$, where D_S and D_{LS} are the observer-source and lens-source angular diameter distances, respectively. The equation (1) is generally non-linear and for a given source position $\vec{\beta}$, one can find multiple possible solutions of $\vec{\theta}$, which define the positions of the images. Their amplification depends on the source and the lens relative position. When it diverges, these source positions form a line named caustic. Meanwhile, the observer perceives these directions of infinite magnification as critical lines. Real sources, which are not point-like but have a certain size, do not experience infinite magnification when they cross a caustic. This is because the amplification is averaged over their entire surface. Caustics and critical lines are usually closed curves and the number of images changes by two when the source crosses them.

If the source is aligned with the lens $\left(\vec{\beta} = 0\right)$, the Einstein's ring (a critical line) is formed with the angular radius θ_E given by,

$$\theta_E = \sqrt{\frac{4GM\left(\theta\right)}{c^2}\frac{D_{LS}}{D_L D_S}}, \tag{2}$$

where *c* is the speed of light, G is the gravitational constant, $M\left(\theta\right)$ is the mass of the lens inside the angle θ and D_L is lens-observer angular diameter distance. Since the scaled lens potential is related to the scaled deflection angle by (Meneghetti, 2021),

$$\vec{\alpha}\left(\vec{\theta}\right) = \vec{\nabla}\Psi\left(\vec{\theta}\right), \tag{3}$$

the lens equation can be written as:

$$\vec{\beta} = \vec{\theta} - \vec{\nabla}\Psi\left(\vec{\theta}\right). \tag{4}$$

The convergence is defined as a dimensionless surface density $\kappa(\theta) = \sum\left(D_L|\theta|\right)/\sum_{crit}$ and $\sum_{crit}$ is the critical surface mass density defined by,

$$\sum_{crit} = \frac{c^2}{4\pi G}\frac{D_S}{D_{LS}D_L}. \tag{5}$$

It is called critical because the condition $\sum \geq \sum_{crit}$ (i.e., $\kappa \geq 1$) is sufficient to produce multiple images for some source positions. For any axisymmetric lens directly in front of a source, an Einstein ring will appear if $\kappa(0) > 1$ (Congdon & Keeton, 2018). Note that the convergence depends not only on the assumed mass distribution of the lens but also on the distances between lens, source, and observer.

Because light rays have a limited propagation speed, it takes a certain amount of time for them to get from a distant source to the observer. There are two reasons why the light experiences a delay when it is lensed by the foreground galaxy. First, because a bent light beam travels a longer distance, it takes more time to propagate (geometric time). Second, due to the time dilation effect induced by general relativity, light rays experience a delay when they traverse a gravitational potential (called gravitational time). The last is the well-known Shapiro effect, which has been highly accurately tested by radar echo delay experiments directed towards the Solar System's inner planets (Shapiro, 1964).

The total time delay $\Delta t = \Delta t_{geom} + \Delta t_{grav}$ is:

$$\Delta t = \frac{1+z_L}{c}\frac{D_L D_S}{D_{LS}}\left[\frac{1}{2}\left(\vec{\theta} - \vec{\beta}\right)^2 - \Psi\left(\vec{\theta}\right)\right] + const\,. \tag{6}$$

Here, z_L is the redshift of the lens. If the source is time variable, the relative time delay between lensed images is potentially an observable quantity. For two images positioned at $\vec{\theta}_1$ and $\vec{\theta}_2$, it can be written as:

$$\Delta t_{1,2} = \frac{1+z_L}{c}\frac{D_L D_S}{D_{LS}}\left[\frac{1}{2}\left(\vec{\theta}_1 - \vec{\beta}\right)^2 - \frac{1}{2}\left(\vec{\theta}_2 - \vec{\beta}\right)^2 - \Psi\left(\vec{\theta}_1\right) + \Psi\left(\vec{\theta}_2\right)\right]. \tag{7}$$

Among the quantities that enter the last equation, only the image positions defined by the angles $\left(\vec{\theta}_1, \vec{\theta}_2\right)$ are directly observed, whereas the lens potential $\Psi\left(\vec{\theta}\right)$ and the source position $\vec{\beta}$ must be inferred via lens modelling.

In Appendices A and B, we have shown two models used frequently for the structure of the galaxies: the Singular Isothermal Sphere (SIS) and Non-singular Isothermal Sphere (NIS) models, respectively. The SIS model has two limitations: the infinite total mass and the central singularity, which do not rule out its use as a galactic lens model. First, the nonzero core radii are typically too small to have a significant impact when compared to the Einstein radius. Second, the multiple lensed images are insensitive to the mass distribution outside the Einstein radius. We consider however the NIS model for the lensing galaxy, which smooths out the central singularity in the SIS model introducing a core region with finite density.

3. Simulations and results

We assume that a strong lensing event is detectable by the telescope if its Einstein angle is higher than the accuracy resolution of the telescope. To investigate the possibility to observe such events we use the Monte Carlo method to extract all needed parameter. Here we list every step in our algorithm (see Hamolli et al., 2023 for more details):

- According to the quasar distribution determined by Schneider et al. (2015), we calculate quasar's redshift.

- To generate the galaxy's redshift, the distribution obtained by Appenzeller et al. (2004) is used, with the restriction that it is smaller than the quasar's redshift. For each quasar, the total number of galaxies satisfying this condition is determined by the cumulative number of galaxies.

- For every galaxy generated, we determine its mass using the stellar mass function Davidzon et. al. (2017). Based on the relation between the galaxy's stellar mass and stellar velocity distribution provided by Zahid et al. (2016), we calculate its velocity dispersion.

- The Einstein angle θ_0 for the quasar/galaxy pair is determined using the SIS model for galaxies (equation (10)), along with the redshifts of the galaxy and quasar. Research on 53 large early-type strong gravitational lens galaxies (Bolton et al., 2008) suggests that the ratio of the stellar velocity dispersion to the velocity dispersion derived from lensing, under the assumption of a SIS

model is approximately one. Therefore, our method of calculating the Einstein radius from equation (10), by substituting the value of σ for σ_{SIS}, seems to be a valid approach.

- For a single galaxy, the probability to reside inside the Einstein angle about the observer–quasar direction would scale as $\theta_0^2/4$. Since, Appenzeller et al., (2004) give the redshift distribution of 7000 galaxies, we normalize the probability considering the whole number of galaxies, 200 billion (0.25 galaxies per arcsec^2, (Beckwith et al., 2006)), and estimate it equal to $10^8\,\theta_0^2/14$. We compare this result with a random number, uniformly distributed in the interval (0, 1), which is extracted by the Monte Carlo code. We keep this pair when its probability is smaller; otherwise, we reject it. The procedure is repeated for all expected quasars to be observed by the Roman Space Telescope.

- For each aligned quasar-galaxy pair, the positions of images and the time delays between them are computed, considering a time-variable quasar.

- Moreover, for the aligned quasar-galaxy pair, we also consider the NIS model for the galaxy. We ask for the quasar-galaxy pair to produce three images, so we generate a random $\theta_c < (1/2)\theta_0$ until it fulfils the condition $\beta < \beta_R$.

- Subsequently, θ_{NIS} is defined, the positions of three images are determined, and the time delays between external images is calculated.

The probability of a quasar being lensed by foreground galaxies is determined by comparing the Einstein angle of the pair with the angular precision of the instrument. For our calculations we have assumed the Universe is flat $(\Omega_k = 0)$ and three angular diameter distances are found by (Liao, 2019):

$$D_L = \frac{c}{H_0(1+z_L)}\int_0^{z_L}\frac{dz}{E(z)},\quad D_S = \frac{c}{H_0(1+z_S)}\int_0^{z_S}\frac{dz}{E(z)},$$

$$D_{LS} = D_S - \frac{1+z_L}{1+z_S}D_L, \tag{25}$$

with

$$E(z)=\sqrt{\Omega_m(1+z)^3+\Omega_k(1+z)^2+\Omega_\lambda}. \quad (26)$$

Here, H_0 is the Hubble constant and Ω_m, Ω_k, Ω_λ are the dimensionless density parameters, i.e. the sum of the cold dark matter and the baryonic matter, the space-curvature, and the dark energy, respectively. The values used for these parameters are as follows: $\Omega_m=0.30$ $\Omega_k=0$, $\Omega_\lambda=0.70$ and $H_0=70\,\mathrm{km\ s^{-1}\ Mpc^{-1}}$.

Based on the algorithm described above, we generate a sample of 100.000 strong lensing events. Assuming the SIS model for the galaxies we find the quasars that will be lensed by foreground galaxies. Considering Roman telescope observation with an angular resolution of 0.11 arcsec we find that around 85% of the lensed quasar are lensed by a single galaxy.

For the lensed quasars by a foreground galaxy, we calculate the position of the two images and time delays between them when the galaxy is characterized by a SIS model. Further on, we calculate the positions of the three real images and the time delays between two external images in case the NIS is assumed. The middle image is not considered in the time delays because it is close to the galaxy and is difficult to observe.

To clearly understand the effects of adding a core radius to the lens galaxy, we have shown in Figure 1. all parameters needed for 30 simulated strong events with largest values of θ_0.

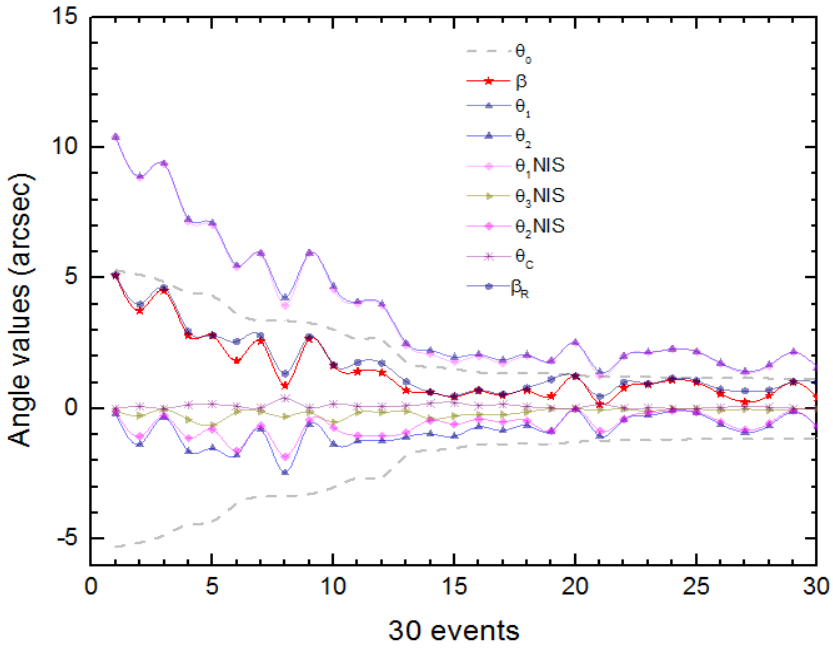

Figure 1. This figure illustrates the angular values (in arcseconds) for 30 strong lensing events with the largest value of θ_0. The dashed grey lines represent the values of θ_0, while the red line indicates the values of β. The blue lines depict the values of θ_1 and θ_2 for the SIS model. The magenta lines illustrate the values of θ_{1NIS} and θ_{2NIS}, which correspond to the external images for the NIS model. The dark yellow line signifies the middle image θ_{3NIS}, the purple line represents the value of the core angle, θ_c and the navy line indicates the radial caustic angle β_R.

The grey lines show the Einstein angle θ_0, the red line depicts the angular positions of the quasar, β, the blue lines show two images (θ_1, θ_2) for the SIS model. The magenta lines illustrate the values of θ_{1NIS} and θ_{2NIS}, which correspond to the external images for the NIS model. The dark yellow line signifies the middle image θ_{3NIS}, the purple line represents the value of the core angle, θ_c and the navy line indicates the radial caustic angle β_R. As it

can be seen, the images of the SIS model are on the two opposite sides of the lens (at the center), with one image inside the Einstein ring (θ_2) and the other outside it (θ_1). In case of the NIS model, a random core angle, $\theta_c < \frac{1}{2}\theta_0$ is generated to fulfil $\beta < \beta_R$. Two external images, θ_{1NIS} and θ_{2NIS} are located closer to each other than the corresponding angles in the SIS model and the θ_{3NIS} is very close to the galaxy center.

The time delays between the lensed images for the SIS (Δt_{SIS}) and the NIS (Δt_{NIS}) models, are calculated. Also, we find the difference ($\Delta t_{SIS} - \Delta t_{NIS}$) between them. In Figure 2. are shown the probability (the ratio of the event number with the time delay in each bin to the total number) of the time delays between two images for each bin of time. The width of each bin is 10 days

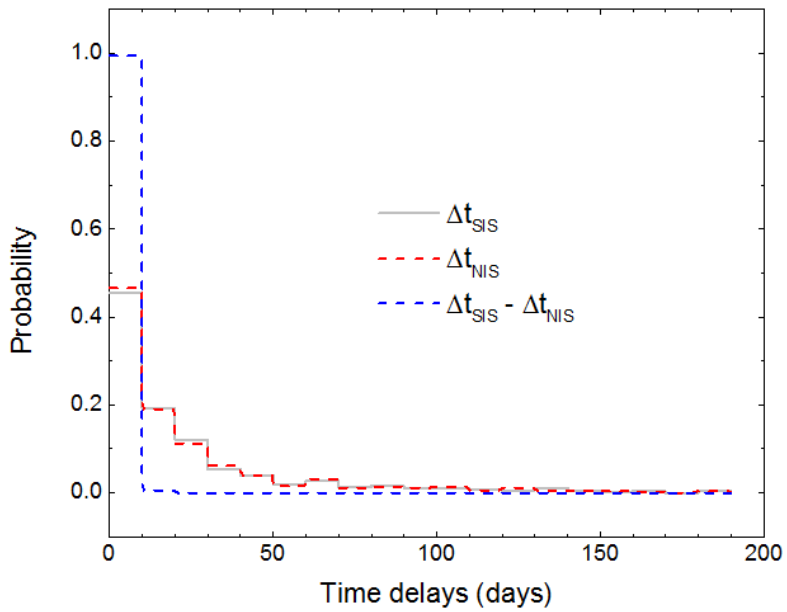

Figure 2. This figure shows the probability of time delays between two images for both the SIS (represented by the grey line) and NIS (depicted by the dashed red line) models. The difference between time delays for two models, $\Delta t_{SIS} - \Delta t_{NIS}$ is shown by the dashed blue line. The width of the bin is 10 days.

In fact, the time delays between two images, range from a minimum of 3.5 hours to a maximum of over 2000 days. To improve the clarity of the plot, 2.5% of the events have been excluded. The median value of the time delays for both the SIS and NIS model is about 11 days. The difference between them, $\Delta t_{SIS} - \Delta t_{NIS}$ range from 0.1 hours to 73 days, with a median value of 7.5 hours.

We further computed the angular separation between images for the SIS model $\Delta\theta_{SIS} = \theta_1 - \theta_2$, as well as the angular separation between external images for the NIS model $\Delta\theta_{NIS} = \theta_{1NIS} - \theta_{2NIS}$. In Figure 3. we plot the variation of the ratio of these two angular separations $\Delta\theta_{SIS}/\Delta\theta_{NIS}$ versus the ratio of the time delays $\Delta t_{SIS}/\Delta t_{NIS}$. As can be observed, there is a linear relationship between them.

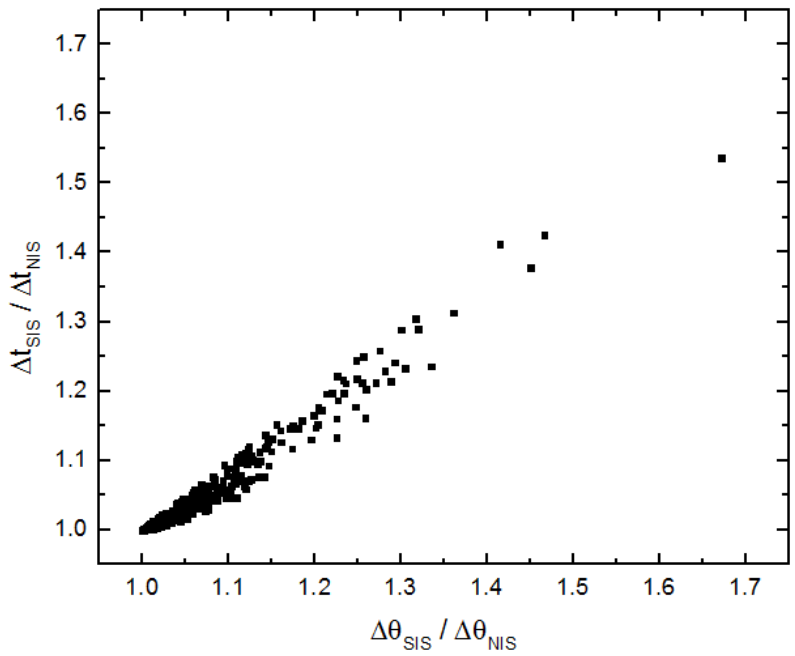

Figure 3. This figure illustrates the variation of the ratio of the time delays $\Delta t_{SIS}/\Delta t_{NIS}$ versus the ratio of the angular separations $\Delta\theta_{SIS}/\Delta\theta_{NIS}$.

Conclusions

In this paper we have explored the influence of the galactic models on the time delays between lensed images in quasars lensed by a single galaxy. The measurement of time delays between images in strong lensing events is crucial for constraining cosmological parameters. Our study is focused on future observations from the Roman telescope.

We find that 85% of lensed quasars will be lensed purely by a galaxy.

As discussed in the previous section, if the quasar is time-variable, the time delay between the lensed images can be calculated using Eq. (7). It is the product of one term, which is inversely proportional to H_0 (each of the angular diameter distance in a flat universe is invers proportional to H_0) and another term that depends on the lens configuration and its mass distribution. Using of the time delay method to constrain cosmological parameters includes several challenges: 1) Modelling uncertainties that may distort the derived parameters; 2) The influence of substructures and the environment on the lensing potential, causing additional time delays; 3) Systematic errors arising from factors such as telescope calibration, model selection, and assumptions about the lensing object; 4) A limited sample size that reduces the validity of the derived parameters. But the feature of the Roman Telescope will soften these limitations with its large field of view and the high sensitivity, enabling the detection of more strong lensing events and increasing the sample size for improved statistical power.

For events expected to be observed by the Roman Telescope we consider only two models: SIS and NIS, because for other models the analytic solution of the lens equation is impossible. Our findings indicate that the highest probability of the time delays between lensed images is around 10 days in both models. In fact, the disparity between these two models is very small because in the SIS model, the time delays are purely gravitational, and the image within the Einstein radius is the most delayed. Conversely, in the NIS model, as the positions of the external images are closer to the galaxy, the gravitational time delay for each image is larger than in the SIS model. The image closer to the galaxy is gravitationally delayed more than the other, but it is geometrically shorter, and the time delays between them changes very little. Therefore, the difference in time delays between the two models does not change significantly. We find also that the ratio of these angular separations $\Delta\theta_{SIS}/\Delta\theta_{NIS}$ is linearly dependent versus the ratio of the time delays $\Delta t_{SIS}/\Delta t_{NIS}$.

Additionally, we investigate the range of the core radii generated for the NIS model of the galaxy and find that they vary from a few parsecs up to several hundred, as predicted by King & Minkowski, (1972).

The process of statistically analysing the time delays between lensed images is crucial for future observational studies. This information is a key resource in designing effective strategies and plans for these upcoming observations.

References

Aghanim, N., Akrami, Y., Ashdown, M., Aumont, J., Baccigalupi, C., Ballardini, M., Banday, A. J., Barreiro, R. B., Bartolo, N., Basak, S., Battye, R. A., Benabed, K., Bernard, J., Bersanelli, M., Bielewicz, P., Bock, J. J., Bond, J. R., Borrill, J., Bouchet, F. R., … Zonca, A. (2020). *Planck*2018 results. *Astronomy and Astrophysics*, *641*, A6.

https://doi.org/10.1051/0004-6361/201833910

Aiola, S., Calabrese, E., Maurin, L., Næss, S., Schmitt, B. L., Abitbol, M. H., Addison, G. E., Ade, P. a. R., Alonso, D., Amiri, M., Amodeo, S., Angile, E., Austermann, J. E., Baildon, T., Battaglia, N., Beall, J. A., Bean, R., Becker, D., Bond, J. R., … Zhu, N. (2020). The Atacama Cosmology Telescope: DR4 maps and cosmological parameters. Journal of Cosmology and Astroparticle Physics, 2020(12), 047. https://doi.org/10.1088/1475-7516/2020/12/047

Appenzeller, I., Bender, R., Böhm, A., Stephan, F., Fricke, K. J., Gabasch, A., Heidt, J., Hopp, U., Jäger, K., Mehlert, D., Noll, S., Saglia, R., Seitz, S., Tapken, C., & Ziegler, B. (2004). Exploring Cosmic Evolution with the FORS Deep Field. The Messenger, 116, 18–24. http://pubman.mpdl.mpg.de/pubman/item/escidoc:949258

Beckwith, S., Stiavelli, M., Koekemoer, A. M., Caldwell, J. a. R., Ferguson, H. C., Hook, R. N., Lucas, R. A., Bergeron, L., Corbin, M. R., Jogee, S., Panagia, N., Robberto, M., Royle, P., Somerville, R. S., & Sosey, M. (2006). The Hubble Ultra Deep field. The Astronomical Journal, 132(5), 1729–1755. https://doi.org/10.1086/507302

Bolton, A., Treu, T., Koopmans, L. V. E., Gavazzi, R., Moustakas, L. A., Burles, S., Schlegel, D. J., & Wayth, R. B. (2008). The Sloan Lens ACS Survey. VII. Elliptical Galaxy Scaling Laws from Direct Observational Mass Measurements. The Astrophysical Journal, 684(1), 248–259. https://doi.org/10.1086/589989

Congdon, A. B., & Keeton, C. R. (2018). Principles of gravitational lensing. In Springer eBooks. https://doi.org/10.1007/978-3-030-02122-1

Davidzon, I., Ilbert, O., Laigle, C., Coupon, J., McCracken, H. J., Delvecchio, I., Masters, D., Capak, P., Hsieh, B. C., Le Fèvre, O., Tresse, L., Bethermin, M., Chang, Y. -Y., Faisst, A. L., Le Floc'h, E., Steinhardt, C., Toft, S., Aussel, H., Dubois, C., Hasinger, G., Salvato, M., Sanders, D. B., Scoville, N., Silverman, J. D. (2017). The COSMOS2015 galaxy stellar mass function. Thirteen billion years of stellar mass assembly in ten snapshots. Astron. Astrophys, 605, A70. https://doi.org/10.1051/0004-6361/201730419

Eigenbrod. A., (2011). Gravitational lensing of quasars. CRC Pres.

Hamolli, L., Hafizi, M., De Paolis, F., Guliqani, E., (2023). Investigating Gravitationally Lensed Quasars Observable by Nancy Grace Roman Telescope. Galaxies 2023, 1, 0. https://doi.org/10.3390/galaxies1010000, https://www.mdpi.com/journal/galaxies.

Hurtado, R. A., Castañeda, L., & Tejeiro, J. M. (2014). Gravitational lensing by spherical lenses. International Journal of Astronomy and Astrophysics, 04(02), 340–352. https://doi.org/10.4236/ijaa.2014.42028

King, I. R., & Minkowski, R. (1972). Mass-Luminosity ratios and sizes of giant elliptical galaxies. Symposium - International Astronomical Union, 44, 87–88. https://doi.org/10.1017/s0074180900005350

Liao, K., (2019). Measuring the Distances to Quasars at High Redshifts with Strong Lensing. The Astrophysical Journal, 883(1), 3. https://doi.org/10.3847/1538-4357/ab39e6

Meneghetti, M., (2021). Introduction to Gravitational Lensing With Python Examples, Lecture notes in Physics. (n.d.). Springer. http://www.springer.com/series/5304

Meylan, G., Jetzer, P., North, P., Schneider, P., Kochanek, C. S., & Wambsganß, J. (2006). Gravitational lensing: strong, weak and micro. In Saas-Fee Advanced Course. https://doi.org/10.1007/978-3-540-30310-7

Mollerach, S., & Roulet, E. (2002). Gravitational lensing and microlensing. World Scientific.

Myers, S., Jackson, N., Browne, I. W. A., De Bruyn, A. G., Pearson, T. J., Readhead, A. C. S., Wilkinson, P. N., Biggs, A. D., Blandford, R. D., Fassnacht, C. D., Koopmans, L. V. E., Marlow, D. R., McKean, J. P., Norbury, M., Phillips, P., Rusin, D., Shepherd, M. C., & Sykes, C. M. (2003). The Cosmic Lens All-Sky Survey - I. Source selection and observations. Monthly Notices of the Royal Astronomical Society, 341(1), 1–12. https://doi.org/10.1046/j.1365-8711.2003.06256.x

Refsdal, S. (1964). On the Possibility of Determining Hubble's Parameter and the Masses of Galaxies from the Gravitational Lens Effect. Monthly Notices of the Royal Astronomical Society, 128(4), 307–310. https://doi.org/10.1093/mnras/128.4.307

Riess, A. G., Casertano, S., Yuan, W., Bowers, J. B., Macri, L. M., Zinn, J., & Scolnic, D. (2021). Cosmic Distances Calibrated to 1% Precision with Gaia EDR3 Parallaxes and Hubble Space Telescope Photometry of 75 Milky Way Cepheids Confirm Tension with ΛCDM. The Astrophysical Journal, 908(1), L6. https://doi.org/10.3847/2041-8213/abdbaf

Schechter, P. The Hubble constant from gravitational lens time delays. (2004) Proc. Int. Astron. Union 2004, 281–296.

Schneider, D. P., Hall, P. B., Richards, G. T., Vanden Berk, D. E., Anderson, S. F., Fan, X., Jester, S., Stoughton, C., Strauss, M. A., SubbaRao, M., Brandt, W. N., Gunn, J. E., Yanny, B., Bahcall, N. A., Barentine, J. C., Blanton, M. R., Boroski, W. N., Brewington, H., Brinkmann, J., … York, D. G. (2005). The Sloan Digital Sky Survey Quasar Catalog. III. Third Data release. The Astronomical Journal, 130(2), 367–380.

https://doi.org/10.1086/431156

Schneider, P., Ehlers, J., & Falco, E. (1992). Gravitational lenses. In Astronomy and astrophysics library. https://doi.org/10.1007/978-3-662-03758-4

Shapiro, I. I. (1964). Fourth test of general relativity. Physical Review Letters, 13(26), 789–791. https://doi.org/10.1103/physrevlett.13.789

Spergel, D. N., Gehrels, N., Baltay, C., Bennett, D. P., Breckinridge, J. B., Donahue, M., Dressler, A., Gaudi, B. S., Greene, T. P., Guyon, O., Hirata, C., Kalirai, J., Kasdin, N. J., Macintosh, B., Moos, W., Perlmutter, S., Postman, M., Rauscher, B. J., Rhodes, J., Zhao, F. (2015). Wide-Field InfrarRed Survey Telescope-Astrophysics Focused Telescope Assets WFIRST-AFTA 2015 Report. arXiv (Cornell University). http://arxiv.org/pdf/1305.5422.pdf

York, D. G., Adelman, J., Anderson, J. E., Anderson, S. F., Annis, J., Bahcall, N. A., Bakken, J. A., Barkhouser, R. H., Bastian, S., Berman, E., Boroski, W. N., Bracker, S., Briegel, C., Briggs, J. W., Brinkmann, J., Brunner, R., Burles, S., Carey, L. N., Carr, M., . . . Pauls, A. G. (2000). The Sloan Digital Sky Survey: Technical Summary. The Astronomical Journal, 120(3), 1579–1587. https://doi.org/10.1086/301513

Wong, K., Suyu, S., Chen, G., Rusu, C., Millon, M., Sluse, D., Bonvin, V., Fassnacht, C., Taubenberger, S., Auger, M., et al. (2020). H0LiCOW–XIII. A 2.4 per cent measurement of H0 from lensed quasars: 5.3 σ tension between early-and late-Universe probes. Mon. Not. R. Astron. Soc. 2020, 498, 1420–1439.

Zahid, H. J., Geller, M. J., Fabricant, D. G., & Hwang, H. S. (2016). THE SCALING OF STELLAR MASS AND CENTRAL STELLAR VELOCITY DISPERSION FOR QUIESCENT GALAXIES ATz< 0.7. The Astrophysical Journal, 832(2), 203. https://doi.org/10.3847/0004-637x/832/2/203

APPENDIX A. SINGULAR ISOTHERMAL SPHERE (SIS)

The mass density distribution for SIS model is:

$$\rho = \frac{\sigma_{SIS}^{\ 2}}{2\pi G r^2}, \tag{8}$$

where σ_{SIS} is one-dimensional velocity dispersion and r is the distance from the center of the spherical mass distribution (Eigenbrod, 2011). The mass of the galaxy inside the angle θ (Mollerach & Roulet, 2002) is:

$$M(\theta) = \frac{\pi \sigma_{SIS}^{\ 2}}{G} \theta D_L . \tag{9}$$

The Einstein angle is given by:

$$\theta_0 = \frac{4\pi {\sigma_{SIS}}^2}{c^2}\frac{D_{LS}}{D_S}. \tag{10}$$

For this model, $\alpha(\theta) = \theta_0 \frac{|\theta|}{\theta}$ and the lens equation (Eq. (18)), takes the form:

$$\theta = \beta + \theta_0 \frac{|\theta|}{\theta}. \tag{11}$$

If $\beta < \theta_0$, the source lies inside the Einstein ring and the lens equation has two solutions:

$$\theta_1 = \beta + \theta_0 \text{ and } \theta_2 = \beta - \theta_0. \tag{12}$$

The two images are on opposite sides of the lens, with one image inside the Einstein ring and the other outside it. The scaled lens potential for SIS can be written as:

$$\Psi(\theta) = \frac{4\pi\sigma^2}{c^2}\frac{D_{LS}}{D_S}|\theta| = \theta_0|\theta|. \tag{13}$$

The time delay between lensed images is,

$$\Delta t_{1,2} = \frac{1+z_L}{2c}\frac{D_L D_S}{D_{LS}}\left(\theta_1^2 - \theta_2^2\right). \tag{14}$$

Appendix B. *Nonsingular Isothermal Sphere (NIS)*

The mass distribution for the NIS model is,

$$\rho(r) = \frac{{\sigma_{SIS}}^2}{2\pi G}\left(\frac{1}{r^2 + r_c^2}\right). \tag{15}$$

The core radius r_c is related to the θ_c, by $r_c = \theta_c D_L$. The mass enclosed inside a circle of radius θ (Mollerach & Roulet, 2002) is given by:

$$M(\theta) = \frac{\pi {\sigma_{SIS}}^2 D_L}{G}\left(\sqrt{\theta^2 + \theta_c^2} - \theta_c\right), \tag{16}$$

and the scale deflection angle by,

$$\alpha(\theta)=\frac{\theta_0}{\theta}(\sqrt{\theta^2+\theta_c^2}-\theta_c). \tag{17}$$

Then, the lens equation for the NIS model looks like this:

$$\vec{\beta}=\vec{\theta}\left(1-\frac{\theta_0}{\theta^2}\left(\sqrt{\theta^2+\theta_c^2}-\theta_c\right)\right), \tag{18}$$

where θ_0 is the Einstein angle for the SIS model. The Einstein angular radius for the NIS model is given by:

$$\theta_{ENIS}=\theta_0\sqrt{1-\frac{2\theta_C}{\theta_0}}, \tag{19}$$

and it can be obtained only for $\theta_c<(1/2)\theta_0$. This condition is the same with that of the convergence. For NIS model the convergence can be written:

$$\kappa(\theta)=\frac{\theta_0}{2\sqrt{\theta^2+\theta_c^2}}, \tag{20}$$

and the condition $\kappa(0)>1$ is fulfil for $\theta_c<(1/2)\theta_0$. As can be seen by Eq. (19), the Einstein angular radius is smaller than the SIS model corresponding quantity. It represents the critical line of the source located at the $\beta=0$. For the NIS model, there is another critical line with angular radius (Mollerach & Roulet, 2002),

$$\theta_R=\sqrt{\theta_0\theta_c}\left[1-\frac{\theta_c}{2\theta_0}\left(1+\sqrt{1+\frac{4\theta_0}{\theta_c}}\right)\right]^{1/2}, \tag{21}$$

which is smaller than the Einstein radius. The corresponding caustic line is a circle with angular radius $\beta_R=\beta(\theta_R)$. The lens equation (Eq. (18)) can be rewritten as a cubic equation:

$$\theta^3-2\beta\theta^2+\left(\beta^2-\theta_0(\theta_0-2\theta_c)\right)\theta-2\beta\theta_0\theta_c=0. \tag{22}$$

This equation has one or three solutions (images) depending on the location of the source. When $\beta>\beta_R$, the equation has only one real solution (image), which is located on the same side of the source. When the source crosses the radial caustic two images appear, one inside and one outside the radial critical

line. So, for the source located inside the caustic, $\beta < \beta_R$ the Eq. (22) has three real solutions (images). The gravitational potential is given by (Mollerach & Roulet, 2002):

$$\Psi(\theta) = \theta_0 \left[\sqrt{\theta^2 + \theta_c^2} - \theta_c \ln\left(\sqrt{\theta^2 + \theta_c^2} + \theta_c \right) \right], \tag{23}$$

and the time delays between two lensed images can be written as:

$$\Delta t_{1,2} = \frac{1+z_L}{c} \frac{D_L D_S}{D_{LS}} \left[\frac{1}{2}\left(\vec{\theta}_1 - \vec{\beta}\right)^2 - \frac{1}{2}\left(\vec{\theta}_2 - \vec{\beta}\right)^2 - \Psi\left(\vec{\theta}_1\right) + \Psi\left(\vec{\theta}_2\right) \right]. \tag{24}$$